


OPEN

Shootins mediate collective cell migration and organogenesis of the zebrafish posterior lateral line system

Akihiro Urasaki^{1,2}, Seiya Morishita¹, Kosuke Naka¹, Minato Uozumi¹, Kouki Abe¹, Liguang Huang¹, Emiko Watase¹, Osamu Nakagawa², Koichi Kawakami³, Takaaki Matsui⁴, Yasumasa Bessho⁴ & Naoyuki Inagaki¹ 

The zebrafish sensory posterior lateral line is an excellent model system to study collective cell migration and organogenesis. *Shootin1* is a cytoplasmic protein involved in neuronal polarization and axon guidance. Previous studies have shown that *shootin1* couples actin filament retrograde flow with extracellular adhesive substrates at the leading edge of axonal growth cones, thereby producing mechanical force for the migration and guidance of axonal growth cones. However, the functions of *shootin* in peripheral cells remain unknown. Here we identified two novel *shootin* family members, *shootin2* and *shootin3*. In zebrafish, *shootin1* and *shootin3* are expressed in the posterior lateral line primordium (PLL) and neuromasts during embryonic development. A *shootin1* mutant displayed a reduced speed of PLL migration, while *shootin1;shootin3* double mutation inhibited cell proliferation in the PLL. Furthermore, our results suggest that *shootin1* and *shootin3* positively regulate the number of neuromasts and the number of cells in deposited neuromasts. Our study demonstrates that shootins mediate collective cell migration of the posterior lateral line primordium and formation of neuromasts in zebrafish.

The lateral line of fish and amphibians is a mechanosensory system that senses directional water movements^{1–3}. It is composed of two major branches, an anterior part that distributes on the head and a posterior part that extends on the trunk and tail. The individual sensory organs that constitute the lateral line, called neuromasts, are rosette shaped organs that contain the sensory hair cells and surrounding supporting cells. In zebrafish, the posterior lateral line is originated from the posterior lateral line primordium (PLL). During lateral line formation, PLL is formed just posterior to the otic vesicle and migrates toward the tail and periodically deposits cell clusters along the embryonic trunk; the cell clusters subsequently differentiate into neuromasts^{1–3}. As these cell behaviors can be observed directly in the living embryo, the zebrafish PLL is an excellent model system for studying collective cell migration and organogenesis^{1–6}.

Collective cell migration of the PLL is regulated by multiple signaling pathways, including chemokine, Wnt and Fgf^{2,3,7–9}. Chemokine Cxcl12a and its receptors Cxcr4b and Cxcr7b are key regulators of PLL migration^{10–15}. The migrating PLL consists of leading and trailing regions¹⁶; the leading cells express Cxcr4b and can respond to Cxcl12a, whereas the trailing cells, which express Cxcr7b, cannot respond to it^{12,13}. Wnt signaling activated in the leading region restricts Cxcr7b expression and Fgf signaling to the trailing region¹⁷. Self-generated Cxcl12a gradients along the PLL are required for proper migration of the PLL^{14,15}. In addition, notch signaling regulates the organogenesis of the PLL system: it acts downstream of Fgf signaling and increases the number of cells in the deposited neuromasts¹⁸. On the other hand, actin and actin-related proteins play key roles in cell morphogenesis

¹Laboratory of Systems Neurobiology and Medicine, Division of Biological Science, Nara Institute of Science and Technology, Ikoma, Nara, 630-0192, Japan. ²Department of Molecular Physiology, National Cerebral and Cardiovascular Center Research Institute, 6-1 Kishibe-Shinmachi, Suita, Osaka, 564-8565, Japan. ³Division of Molecular and Developmental Biology, National Institute of Genetics, and Department of Genetics, SOKENDAI (The Graduate University for Advanced Studies), Mishima, Shizuoka, 411-8540, Japan. ⁴Laboratory of Gene Regulation Research, Division of Biological Science, Nara Institute of Science and Technology, Ikoma, Nara, 630-0192, Japan. Correspondence and requests for materials should be addressed to N.I. (email: ninagaki@bs.naist.jp)

Received: 6 June 2018

Accepted: 7 August 2019

Published online: 21 August 2019

and migration as readouts of various signaling pathways^{19–22}. However, the molecular mechanics underlying PLLP migration and neuromast formation remain unclear.

Actin filaments (F-actins) polymerize at the leading edge of the motile cells and depolymerize proximally, which, in conjunction with myosin II activity, induces retrograde flow of F-actins^{23–25}. Shootin1²⁶, recently renamed shootin1a²⁷, is a “clutch” molecule involved in neuronal polarization and axon guidance^{26,28–30}. In cultured rat hippocampal neurons, shootin1a accumulates at the leading edge of axonal growth cones (Supplementary Fig. S1)²⁶. It couples mechanically the F-actin retrograde flow (red arrow, Supplementary Fig. S1) and extracellular adhesive substrates, a process called clutch coupling, thereby transmitting the force of F-actin flow (red arrow) to the substrates as a traction force (white arrow)^{31,32}. The driving force for growth cone advance (blue arrow) is produced as a counterforce to the traction forces exerted on the substrate (white arrow). In addition, the growth cone chemoattractant netrin-1 positively regulates shootin1a-mediated clutch coupling, through Pak1-mediated shootin1a phosphorylation, for axon outgrowth and guidance^{33,34}. This coupling also contributes to the intracellular transport of actin and actin-binding proteins toward the leading edge of axons^{35,36}. In addition to neuron-specific shootin1a, a splicing isoform shootin1b is produced from the *shootin1* gene, which is expressed both in the brain and in peripheral tissues²⁷. A recent study reported that shootin1b-mediated clutch coupling produces force for migration of mouse olfactory interneurons³⁷. In zebrafish, a homolog of mammalian *shootin1* has been reported in the genome²⁶ whose expression is upregulated in the brain and peripheral tissues by knock-down of semaphorin or plexin³⁸. However, the functions of shootin in peripheral cells are unknown.

In the present study, we identified two novel shootin family members, shootin2 and shootin3. We demonstrate that the three shootins are present in zebrafish; all of them interact with F-actin retrograde flow, suggesting that these proteins may function as clutch molecules. In addition, we show that *shootin1* and *shootin3* are expressed in the PLLP and neuromasts of zebrafish embryos. Loss of *shootin1* and *shootin3* reduced the speed of primordium migration, the number of neuromasts and the number of cells in deposited neuromasts. The *shootin1;shootin3* double mutation also inhibited cell proliferation in the PLLP. Overall, our findings indicate that shootins are involved in collective cell migration and formation of neuromasts during development of the zebrafish posterior lateral line system.

Results

Identification of novel shootin genes *shootin2* and *shootin3*. Shootin1a was originally identified in cultured rat hippocampal neurons²⁶. Homologs of the rat *shootin1* gene have been identified in human, mouse and zebrafish genomes^{26,38}. Here, we identified, by homology search analysis, two predicted shootin1-like proteins in zebrafish (XP_690881.3 and XP_685212.4). To analyze shootin1 and shootin1-like proteins in zebrafish embryos, we cloned their cDNAs. These cDNAs encode 544-, 561-, and 655-amino acid (aa) proteins that share high similarity with mouse shootin1a (Fig. 1a and Supplementary Fig. S2). Phylogenetic and synteny analyses revealed that shootins are clustered into three separate groups and that the gene encoding the 544-aa protein is orthologous to human *shootin1* (Supplementary Fig. S3a,b). We designated the genes encoding 561- and 655-aa proteins as *shootin2* and *shootin3*, respectively (Fig. 1a and Supplementary Fig. S2). The zebrafish *shootin1*, *shootin2* and *shootin3* genes are located on chromosome 17, 7 and 14, respectively (Supplementary Fig. S3b). Rat shootin1a is phosphorylated at Ser101 and Ser249 by Pak1 and these phosphorylations promote axon outgrowth^{32,33}. The putative phosphorylation site corresponding to Ser101 is present in all the three zebrafish shootin proteins, whereas that corresponding to Ser249 is present in shootin1 and shootin3 but not in shootin2 (arrowheads, Supplementary Fig. S2).

Shootin1-homologous sequences were identified widely in vertebrates, including fish, frogs, reptiles, birds, marsupials and mammals (Supplementary Fig. S3a). Shootin2-homologous sequences were identified in fish, frog and Tasmanian devil (marsupial) but not in placental (eutherian) mammals (Supplementary Fig. S3a). In contrast, shootin3-homologous sequences were identified in fish, such as cavefish, medaka, fugu and coelacanth, but not in other vertebrate lineages (Supplementary Fig. S3a). Because a whole-genome duplication event occurred in the teleost lineage^{39–43}, two orthologs of a gene are often identified in the zebrafish genome, whereas a single copy of the corresponding gene is present in the human genome. Synteny analysis showed that the locus containing zebrafish *shootin1* is conserved widely in vertebrates, such as human, mouse, Tasmanian devil, *Xenopus* and zebrafish (Supplementary Fig. S3b), whereas the locus containing zebrafish *shootin2* is conserved in Tasmanian devil, *Xenopus* and zebrafish (Supplementary Fig. S3b). The orders of genes in the loci containing *shootin2* and *shootin3* were different from those in the loci containing *shootin1*, suggesting that shootin2 and shootin3 are novel shootin family members.

***shootin1* and *shootin3* are expressed in the zebrafish lateral line system.** To examine whether the shootin family members are expressed in developing zebrafish embryos, we performed RT-PCR using specific primers. All three shootin genes were expressed at 24 h post-fertilization (hpf) and 48 hpf (Fig. 1b). The transcripts of *shootin1* and *shootin3* were detected at 0 hpf, while we could not detect *shootin2* at 0 hpf. Whole-mount *in situ* hybridization detected all the three shootin genes expressed in the anterior region of embryos at 36 hpf (Fig. 1c–e). In addition, *shootin1* and *shootin3* were expressed in the neuromasts (arrowheads, Fig. 1c,c’,e,e’) and the PLLP (arrows, Fig. 1c,c’,e,e’) of the lateral line system.

Zebrafish shootins interact with F-actin retrograde flow at the cellular leading edge. Previous speckle imaging analyses *in vitro* showed that shootin1a interacts with F-actin retrograde flow at the leading edge of axonal growth cones, and demonstrated that the shootin1a–F-actin interaction promotes growth cone migration^{31,32} (Supplementary Fig. S1). We next examined whether the zebrafish shootins interact with F-actin retrograde flow. The speckle imaging assay is a useful method to monitor the retrograde flows of F-actin and clutch molecules^{32,44}. As speckle imaging analysis of F-actin flow *in vivo* is technically difficult, we examined shootin

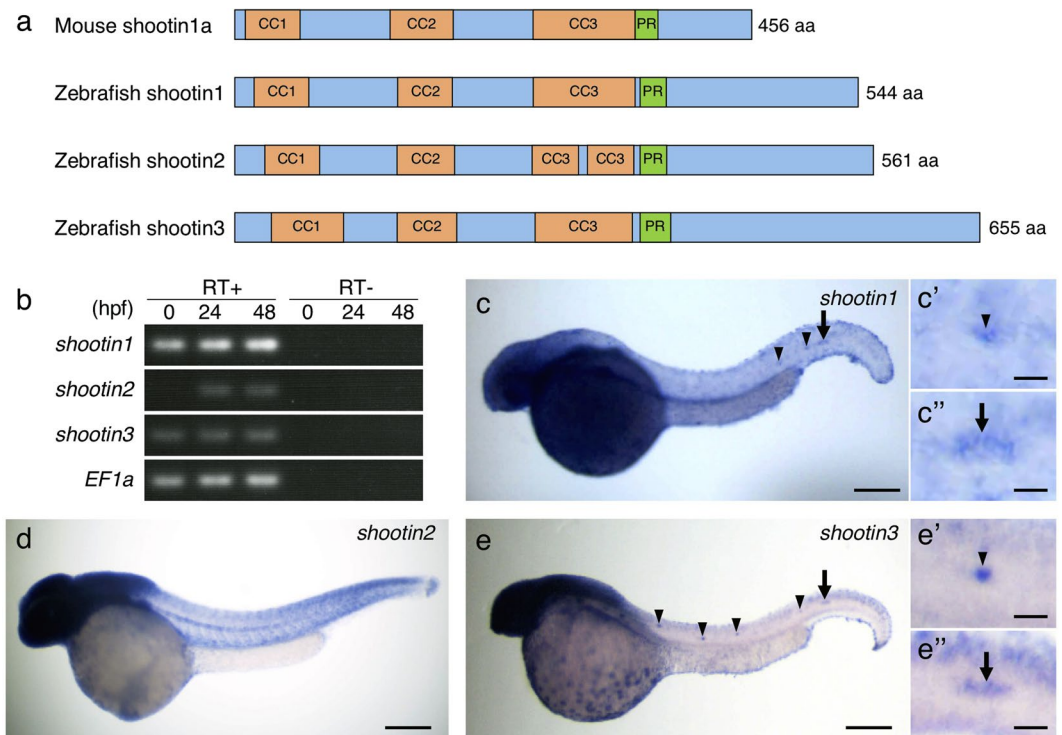


Figure 1. Identification and expression of zebrafish shootin genes. **(a)** Schematic representation of zebrafish shootin1, shootin2, shootin3 and mouse shootin1 protein structures. The top box for mouse shootin1 indicates the structural domains described previously²⁶, and the bottom three boxes for zebrafish shootin1, shootin2 and shootin3 indicate the corresponding structural domains. CC1-3, coiled-coil domains 1-3; PR: proline-rich domain. **(b)** RT-PCR analysis of *shootin1*, *shootin2* and *shootin3* transcripts. Elongation factor 1a (EF1a) was used as a control. Developmental stages are denoted in hours post-fertilization (hpf). RT-PCR products produced in the presence (RT+) or absence (RT-) of reverse transcriptase were electrophoresed using a 3% agarose gel. **(c-e)** Whole-mount *in situ* hybridization of *shootin1* (**c**), *shootin2* (**d**) and *shootin3* (**e**) in zebrafish embryos at 36 hpf. Arrowheads and arrows indicate neuromasts and PLLP, respectively. Enlarged images indicate expression of *shootin1* and *shootin3* in the last deposited neuromasts (**c'** and **e'**) and the PLLP (**c''** and **e''**). Scale bars: 200 μm for whole body images and 25 μm for enlarged images.

dynamics using cultured XTC fibroblasts, a cell line established from *Xenopus laevis*⁴⁵. XTC fibroblasts bear large and thin lamellipodia, and are thus particularly suitable for speckle imaging of the retrograde flows of F-actin and clutch molecules^{32,44}. AcGFP-shootin1 and mRFP-actin were coexpressed in XTC fibroblasts; speckle imaging was performed as described³¹. The AcGFP-shootin1 signals moved retrogradely in the lamellipodia of XTC fibroblasts (Fig. 2a and Movie 1), as reported in the case of mammalian shootin1a³¹. Speckles of AcGFP-shootin1 moved with those of mRFP-actin at a similar speed (AcGFP-shootin1: $1.56 \pm 0.09 \mu\text{m}/\text{min}$, $n = 51$ speckles; mRFP-actin: $1.57 \pm 0.09 \mu\text{m}/\text{min}$, $n = 51$ speckles; Fig. 2a,d, Movie 1). Speckles of AcGFP-shootin2 and AcGFP-shootin3 also underwent retrograde movement at the leading edge of XTC fibroblasts. The speed of AcGFP-shootin2 speckles was similar to that of mRFP-actin speckles (AcGFP-shootin2: $1.48 \pm 0.11 \mu\text{m}/\text{min}$, $n = 54$ speckles; mRFP-actin: $1.46 \pm 0.11 \mu\text{m}/\text{min}$, $n = 54$ speckles; Fig. 2b,d, Movie 2); the AcGFP-shootin3 speckles also moved with mRFP-actin at a similar speed (AcGFP-shootin3: $1.51 \pm 0.11 \mu\text{m}/\text{min}$, $n = 53$ speckles; mRFP-actin: $1.52 \pm 0.09 \mu\text{m}/\text{min}$, $n = 53$ speckles; Fig. 2c,d, Movie 3). These results indicate that zebrafish shootin1, shootin2 and shootin3 interact with F-actin retrograde flow at the cellular leading edge.

Zebrafish shootin1 mediates PLLP migration. The interactions of zebrafish shootin family members with F-actin retrograde flow in XTC fibroblasts raise the possibility that shootin1 and shootin3 mediate the migration of the posterior lateral line system. To assess the functions of shootin1 and shootin3 in the posterior lateral line, we generated *shootin1* and *shootin3* mutants using the CRISPR/Cas9 system. The *shootin1* mutant allele contained an 8-bp deletion in the third exon, resulting in a frame shift and a premature stop codon after 47 aa (Fig. 3a and Supplementary Fig. S4a,b). The *shootin3* mutant allele harbored a 13-bp deletion in the second exon, resulting in a premature stop codon after 26 aa (Fig. 3a and Supplementary Fig. S5a,b). We identified *shootin1* mutants by PCR-based genotyping (Supplementary Fig. S4c) and *shootin3* mutant fish by T7 endonuclease I (T7EI)-based genotyping (Supplementary Figs S5c and S6), respectively. To visualize the PLLP, we crossed the fish with SAIGFF213A;UAS:GFP transgenic fish that express GFP in the PLLP⁴⁶. Consistent with a previous report⁴⁷, during 32–38 hpf, PLLP migrated at $88 \pm 2 \mu\text{m}/\text{h}$ in control embryos ($n = 21$) (Movie 4, Fig. 3b). PLLP also migrated in the *shootin1* mutant embryos (Movie 5, Fig. 3b); however, the migration speed was significantly slower

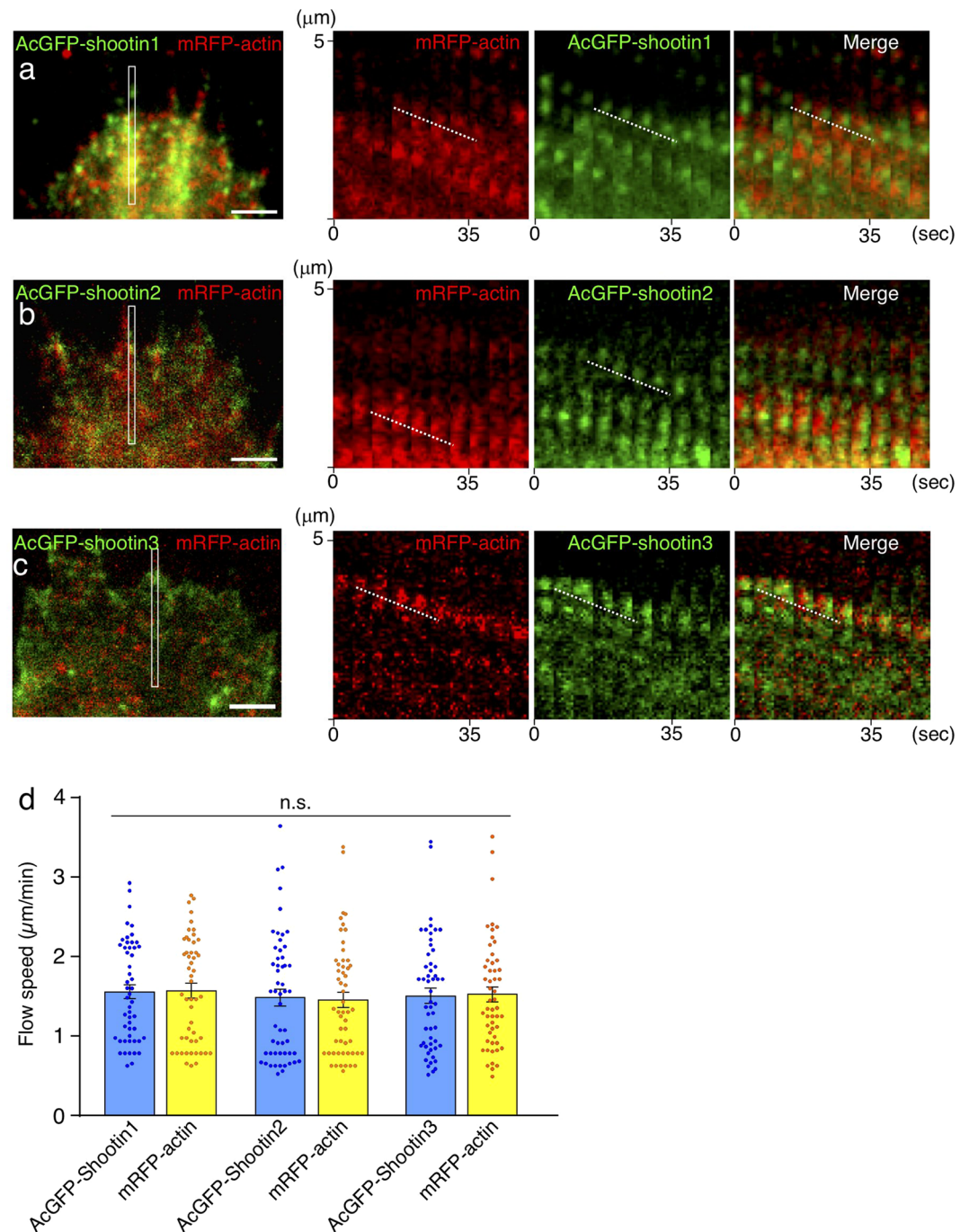


Figure 2. Zebrafish *shootin1*, *shootin2* and *shootin3* interact with F-actin retrograde flow. (a–c) Fluorescent speckle images of AcGFP-*shootin1* (a), AcGFP-*shootin2* (b) and AcGFP-*shootin3* (c) with mRFP-actin in XTC fibroblasts (see Movies 1–3). Kymographs (right) of the areas indicated by rectangles in the left panels show that the fluorescent features of AcGFP-*shootin* and those of mRFP-actin moved at similar speed (dotted lines). (d) Retrograde flow speeds of *shootin1* ($n = 51$ speckles), *shootin2* ($n = 54$ speckles), *shootin3* ($n = 53$ speckles) and F-actin ($n = 107$ speckles) measured from the kymograph analysis in (a–c). Scale bars: 2 μm .

than that in the control embryos (Fig. 3c). On the other hand, no significant difference in the migration speed of PLLP was detected between control and *shootin3* mutant embryos (Movies 4 and 6, Fig. 3b,c).

We also generated a *shootin1;shootin3* double mutant. As in the case of *shootin1* single mutant, the PLLP migration speed was significantly lower than that in control embryos and *shootin3* single mutant embryos (Movies 4, 6 and 7, Fig. 3b,c). When *shootin1* and *shootin3* mRNAs were injected into the double mutant embryos, the reduced speed of PLLP migration was rescued to a level similar to that in the control embryos (Fig. 3b,d). Injection of *shootin1* mRNA into the *shootin1* single mutant embryos also rescued the reduced speed of PLLP migration (Supplementary Fig. S7). The migrating PLLP consists of leading and trailing regions¹⁶; *Cxcr4b* is expressed in

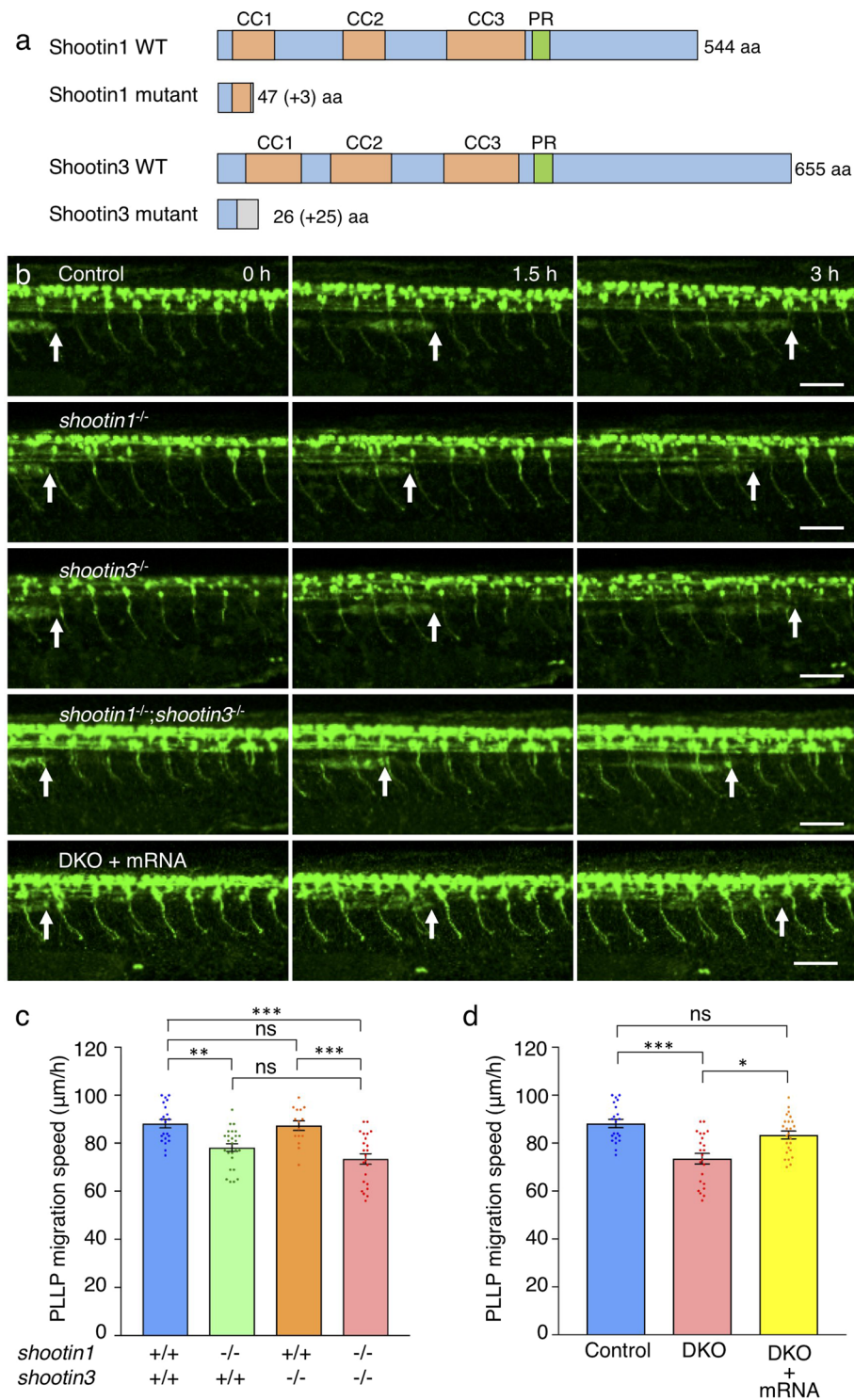


Figure 3. *shootin1* mutants display reduced migration speed of the PLLP. **(a)** Schematic structures of *shootin1* and *shootin3* proteins of the *shootin1* and *shootin3* single mutants. Frameshift mutations in *shootin1* and *shootin3* resulted in premature stop codons after amino acid positions 47 and 26, respectively. The gray boxes indicate amino acids added by the frameshift mutations; numbers in brackets indicate the numbers of these additional residues. CC1-3: coiled-coil domain; PR: proline-rich domain. **(b)** Representative time-lapse images of wild-type control, *shootin1^{-/-}* single mutant, *shootin3^{-/-}* single mutant and *shootin1^{-/-};shootin3^{-/-}* double mutant embryos carrying the SAIGFF213A;UAS:GFP construct. Time-lapse images of a *shootin1^{-/-};shootin3^{-/-}* double mutant embryo into which *shootin1* and *shootin3* mRNAs were injected are also presented at the bottom. Arrows indicate the leading edges of PLLPs. Scale bars: 50 µm. **(c)** Migration speeds of PLLP in wild-type control ($n = 21$), *shootin1^{-/-}* single mutant ($n = 26$), *shootin3^{-/-}* single mutant ($n = 15$) and *shootin1^{-/-};shootin3^{-/-}* double mutant ($n = 23$) embryos at 32–38 hpf obtained from the analyses in **(b)**. **(d)** Rescue analyses of the PLLP migration in the *shootin1;shootin3* double mutants. *shootin1* and *shootin3* mRNAs

were injected into the *shootin1*^{-/-};*shootin3*^{-/-} double knockout (DKO) mutant embryos (DKO + mRNA, $n = 25$). Data for the uninjected wild-type (WT) and DKO mutant embryos in (d) are shared with those in (c). Data for (c) and (d) represent mean \pm SEM. Statistical significance of the differences is indicated with asterisks (*** $P < 0.01$; ** $P < 0.02$; * $P < 0.05$; ns, nonsignificant).

all the cells of the PLLP, whereas *Cxcr7b* is expressed exclusively in the trailing cells¹. We further examined the polarity of PLLP in mutant embryos, using *Cxcr4b* and *Cxcr7b* as markers. As shown in Supplementary Fig. S8a, *cxcr4b* was expressed widely in the wild-type PLLP, whereas *cxcr7b* was expressed only in the trailing region. Their expression patterns in the *shootin1*;*shootin3* double mutant PLLP were similar to those in the wild-type PLLP, suggesting that PLLP polarity was not affected by the *shootin1*;*shootin3* double mutation. Taking these data together, we conclude that *shootin1* plays a key role in PLLP migration.

Shootin1 and shootin3 mediate neuromast formation. Next, we analyzed the number of neuromasts in control and mutant fish after PLLP migration (48 hpf) (Fig. 4). Consistent with previous reports^{17,47}, the average number of neuromasts was 5.4 ± 0.1 ($n = 15$ embryos) in control embryos, and it was significantly reduced by *shootin1* and *shootin3* single mutations (Fig. 4a,b). The number of neuromasts was further decreased in the *shootin1*;*shootin3* double mutants (Fig. 4a,b). Moreover, the injection of *shootin1* and *shootin3* mRNAs rescued significantly the reduced number of neuromasts in the double mutants (Fig. 4a,c). We further counted the number of cells in the first deposited neuromasts at 32 hpf by DAPI staining^{18,48,49} (Fig. 4d). In control embryos, the number of cells detected in the neuromasts was 27.2 ± 0.8 ($n = 14$ neuromasts), which is similar to the previously reported number¹⁸. The *shootin1*;*shootin3* double mutants exhibited a reduced number of neuromast cells, although no significant differences were observed between the control and single mutants (Fig. 4d,e). Furthermore, the injection of *shootin1* and *shootin3* mRNAs rescued partially the reduced cell number in the double mutants (Fig. 4d,f). These data indicate that *shootin1* and *shootin3* mediate neuromast formation, by positively regulating both the neuromast number and the number of cells in neuromasts.

***shootin1*;*shootin3* double mutation reduces cell proliferation in the PLLP.** To investigate how *shootin1* and *shootin3* mediate neuromast formation, we quantified the number of cells in the PLLP at 32 hpf using DAPI staining^{18,48,49} (Fig. 5a). In control embryos, the number of cells detected in the PLLP was 96.6 ± 3.1 ($n = 10$ PLLPs), which is consistent with previous data¹⁸. Although no significant differences were observed in the mean cell numbers in the PLLP between the control and *shootin1* single mutant fish, the *shootin1*;*shootin3* double mutants displayed significantly reduced PLLP cell numbers compared with the control (Fig. 5a,b). We also found that the average number of cells in the double mutant PLLP increased following the injection of *shootin1* and *shootin3* mRNAs (Fig. 5a,c). We further analyzed the PLLP cell number before the first neuromast deposition (24 hpf). In control embryos, the number of cells detected in the PLLP was 125.6 ± 2.7 ($n = 7$ PLLPs). As shown in Supplementary Fig. S9, the cell numbers of the single and double mutant PLLP were similar to those of the wild-type PLLP at 24 hpf.

As previous studies have shown that cells in the migrating PLLP proliferate^{47,50,51}, we next analyzed cell proliferation by EdU labelling (Fig. 5d). The ratio of EdU-positive proliferating cells to the total number of cells in the PLLP was $26.7 \pm 1.9\%$ ($n = 11$ PLLPs) (Fig. 5d,e). The ratio of EdU-positive proliferating cells was reduced significantly by the *shootin1*;*shootin3* double mutation (Fig. 5d,e). We finally analyzed cell fate determination of hair cells by examining the expressions of their markers *atoh1a* and *deltaA*^{1,3}. Expressions of *atoh1a* and *deltaA* in the PLLP and first deposited neuromast were detected in wild-type and *shootin1*;*shootin3* double mutant embryos (Supplementary Fig. S8b). Their expression patterns in the double mutant were similar to those in the wild-type embryo, suggesting that hair cell fate determination was not affected by the *shootin1*;*shootin3* double mutation. Together, these data suggest that *shootin1* and *shootin3* positively regulate cell proliferation in the migrating PLLP.

Discussion

We report here two novel *shootin* family members, *shootin2* and *shootin3*. Phylogenetic analyses identified *shootin1* in a wide range of vertebrates, including eutherians, marsupials, birds, reptiles, amphibians and fish. *Shootin2* was found in marsupial, frog and fish genomes, while *shootin3* is restricted to the fish lineage. Zebrafish *shootin1* and *shootin3* were expressed in the PLLP and neuromasts. The mutation in *shootin1* reduced the speed of primordium migration, while *shootin1*;*shootin3* double mutation led to reduction in cell proliferation in the primordium, neuromast number and number of cells in the neuromasts. Together, these results demonstrate key roles of *shootins* in collective cell migration and neuromast formation of the zebrafish posterior lateral line system.

Concerning the mechanism for *shootin1*-mediated PLLP migration, our data indicate that zebrafish *shootin1* interacts with F-actin retrograde flow at the leading edge of fibroblasts. Previous studies reported that rat *shootin1a* interacts with F-actin retrograde flow at the leading edge of axonal growth cones, thereby producing force for growth cone migration as a clutch molecule (Supplementary Fig. S1)^{31–33}. A recent study also demonstrated that mouse *shootin1b* produces force for neuronal migration through its interaction with F-actin retrograde flow³⁷. In the zebrafish PLLP, F-actin accumulates at the leading edge of the leader cells during collective cell migration⁵². Thus, we consider that zebrafish *shootin1* is likely to mediate PLLP migration by interacting with F-actin at the leading edge of the leader cells (Fig. 6a,b). Although *shootin3* interacted with F-actin retrograde flow, the *shootin3* mutation did not have a significant effect on PLLP migration. However, we do not rule out the possibility that *shootin3* functions as a clutch molecule. As a possible reason to explain the difference between the phenotypes of *shootin1*^{-/-} and *shootin3*^{-/-} fish, the efficiency of *shootin3*-mediated clutch coupling may be weaker than that of *shootin1*-mediated clutch coupling. Alternatively, the expression level of *shootin3* in PLLP may be lower than that of *shootin1*.

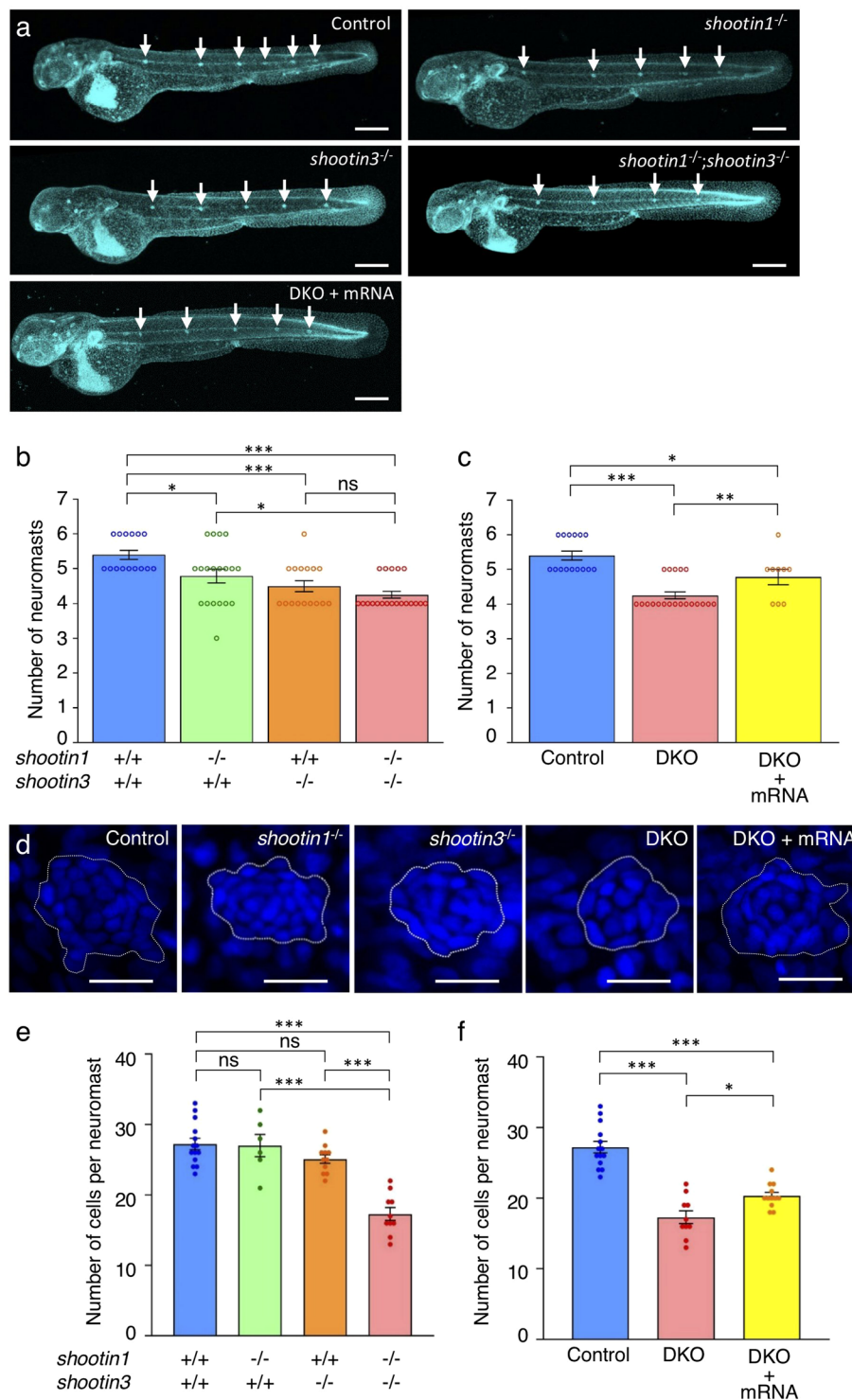


Figure 4. *shootin1;shootin3* double mutants exhibit reduced number of neuromasts and reduced number of cells in neuromasts. **(a)** Representative images of wild-type control, *shootin1*^{-/-} single mutant, *shootin3*^{-/-} single mutant and *shootin1*^{-/-};*shootin3*^{-/-} double mutant embryos at 48 hpf. An image of a *shootin1*^{-/-};*shootin3*^{-/-} double mutant embryo into which *shootin1* and *shootin3* mRNAs were injected is also presented at the bottom. Embryos were stained with DAPI. Scale bars: 300 μ m. **(b)** The number of neuromasts obtained from the analyses in **(a)**. The neuromast numbers of wild-type control ($n = 15$), *shootin1*^{-/-} single mutant ($n = 19$), *shootin3*^{-/-} single mutant ($n = 16$) and *shootin1*^{-/-};*shootin3*^{-/-} double mutant ($n = 20$) embryos were counted at 48 hpf. **(c)** Rescue experiments of the reduced number of neuromasts in the *shootin1;shootin3* double mutants. Injected DKO embryos (DKO + mRNA, $n = 9$) were observed at 48 hpf. Data for the uninjected wild-type (WT) and DKO mutant embryos in **(c)** are shared with those in **(b)**. **(d)** Representative images of the DAPI-stained first deposited neuromasts in wild-type control, *shootin1*^{-/-} single mutant, *shootin3*^{-/-} single mutant and *shootin1*^{-/-};*shootin3*^{-/-} double mutant embryos at 32 hpf. An image

of a neuromast in *shootin1*^{-/-};*shootin3*^{-/-} double mutant embryo into which *shootin1* and *shootin3* mRNAs were injected is also shown to the right. Dotted lines indicate the areas of neuromasts, in which small nuclei of neuromast cells cluster. Scale bars: 20 μm. (e) The number of cells in the first deposited neuromasts obtained from the analyses in (d). Wild-type control (*n* = 14), *shootin1*^{-/-} single mutant (*n* = 6), *shootin3*^{-/-} single mutant (*n* = 11), and *shootin1*^{-/-};*shootin3*^{-/-} double mutant (*n* = 10) embryos were analyzed at 32 hpf. (f) Rescue experiments of the reduced cell number of the double mutant neuromasts. Injected DKO embryos (DKO + mRNA, *n* = 12) were observed at 32 hpf. Data for the uninjected wild-type (WT) and DKO mutant embryos in (f) are shared with those in (e). Data in (b,c,e and f) represent mean ± SEM; ****P* < 0.01; **P* < 0.05; ns, nonsignificant.

PLLP migration is regulated by the extracellular signal Cxcl12a and its receptors Cxcr4b and Cxcr7b^{10–15}. In previous reports, we demonstrated that the extracellular chemoattractant netrin-1 induces PAK1-mediated shootin1a phosphorylation at Ser101 and Ser249 in the axonal growth cones; this in turn enhances the coupling between F-actin retrograde flow and cell adhesion, thereby promoting growth cone migration^{32–34}. Interestingly, phosphorylatable serine residues corresponding to these sites are present in zebrafish shootin1, raising a possibility that PLLP migration may be positively regulated by phosphorylation at these sites under chemoattractant signals. Elucidating the detailed molecular mechanisms involved in shootin1-mediated PLLP migration remains an important issue for future investigation.

The present study demonstrated that the number of neuromasts as well as the number of cells in neuromasts were reduced in the *shootin1*;*shootin3* double mutant embryos. As the effect of the *shootin1*;*shootin3* double mutation was larger than that of *shootin1* single mutation or *shootin3* single mutation, we think that shootin1 and shootin3 up-regulate cooperatively the neuromast number and the number of cells in neuromasts. Concerning these results, our data also showed that the *shootin1*;*shootin3* double mutation inhibits cell proliferation in the PLLP, suggesting that shootin1 and shootin3 promote cell proliferation there. Although the molecular mechanisms underlying the shootin-mediated cell proliferation are unclear, we expect that the increased cell proliferation in the PLLP positively regulates both the number of neuromasts and the number of cells in neuromasts (Fig. 6a). The details of how neuromast formation is regulated by shootin1 and shootin3 remain for further analyses.

Methods

Zebrafish and husbandry. All relevant aspects of the experimental procedures were approved by the Institutional Animal Care and Use Committee of Nara Institute of Science and Technology (reference No. 1321) and carried out in accordance with relevant guidelines and regulations. Wild type and the SAIGFF213A line⁴⁶ were used in this study. Zebrafish were maintained under standard husbandry conditions at 28.5 °C with a 14 h light and 10 h dark cycle.

Cloning of zebrafish shootin cDNAs. Total RNA was purified from zebrafish embryos using TRIzol reagent (Invitrogen), according to the manufacturer's instructions. The RNA sample was used to synthesize cDNA with MLV RT (H-) Point Mutant (Promega) using primer AP (Supplementary Table S1) for reverse transcription. Specific cDNAs were PCR-amplified using the following primers: shootin1-h-Ba-Ko and shootin1-t-Xb-No for shootin1, shootin2-h-Ba-Ko and shootin2-t-Xb-No for shootin2, and shootin3-h-Ba-Ko and shootin3-t-Sp for shootin3 (Supplementary Table S1). The shootin1 and shootin2 fragments were digested with BamHI and XbaI restriction endonucleases, whereas shootin3 fragments were digested with BamHI and SpeI. The cDNAs were then cloned into the BamHI-XbaI site of pCS2 and sequenced using an ABI PRISM 3130 (Applied Biosystems).

Vector construction. pCS2-EGFP-shootin1 was constructed as follows. pCS2-MCS was first constructed by self-ligating the PCR product amplified from pCS2 using the primers pCS2-5'-out-Ba and pCS2-3'-out-Ba-Sp-Bg-Xb (Supplementary Table S1), and digesting with BamHI. pCS2-EGFP was constructed by replacing a short BamHI-SpeI fragment of pCS2-MCS with the EGFP gene fragment PCR-amplified from pT2AL200R150G⁵³ using the primers EGFP-h-Bg-Ko and EGFP-t-Sp (Supplementary Table S1), and digesting with BamHI and SpeI. Finally, pCS2-EGFP-shootin1 was constructed by replacing a short BglII-XbaI fragment of pCS2-EGFP with the shootin1 gene fragment amplified from shootin1 cDNA using the primers shootin1-h-Ba and shootin1-t-Xb-No (Supplementary Table S1), and digesting with BamHI and XbaI. pCS2-EGFP-shootin2 and pCS2-EGFP-shootin3 were constructed in a similar manner to pCS2-EGFP-shootin1, using primers shootin2-h-Ba and shootin2-t-Xb-No for shootin2, and primers shootin3-h-Ba and shootin3-t-Sp for shootin3 (Supplementary Table S1). For constructing pAcGFP-shootin1, a short BamHI-SalI fragment of pAcGFP-C1 (Clontech) was replaced with the shootin1 gene fragment, which was amplified from *shootin1* cDNA using shootin1-h-Ba and shootin1-t-Sa primers (Supplementary Table S1), and digested with BamHI and SalI. pAcGFP-shootin2 and pAcGFP-shootin3 were constructed in a similar manner to pAcGFP-shootin1, using shootin2-h-Ba and shootin2-t-Sa primers for *shootin2*, and shootin3-h-Ba and shootin3-t-Sa primers for *shootin3* (Supplementary Table S1).

Identification of shootin genes and phylogenetic analysis. Shootin family members were identified in the zebrafish genome using BLAST analysis. Multiple alignments and phylogenetic analysis were performed using Genetyx ver.13 (Genetyx). The coiled-coil domains of shootin proteins were predicted using SMART⁵⁴. The phylogenetic tree was constructed using the neighbor-joining method⁵⁵.

RT-PCR. To analyze the expression of shootin family members during zebrafish development, RT-PCR was performed using shootin1-rt-f and shootin1-rt-r primers for shootin1, shootin2-rt-f and shootin2-rt-r primers for shootin2, and shootin3-rt-f and shootin3-rt-r primers for *shootin3*. We used EF1a-rt-f and EF1a-rt-r primers as a positive control. The primers used are listed in Supplementary Table S1.

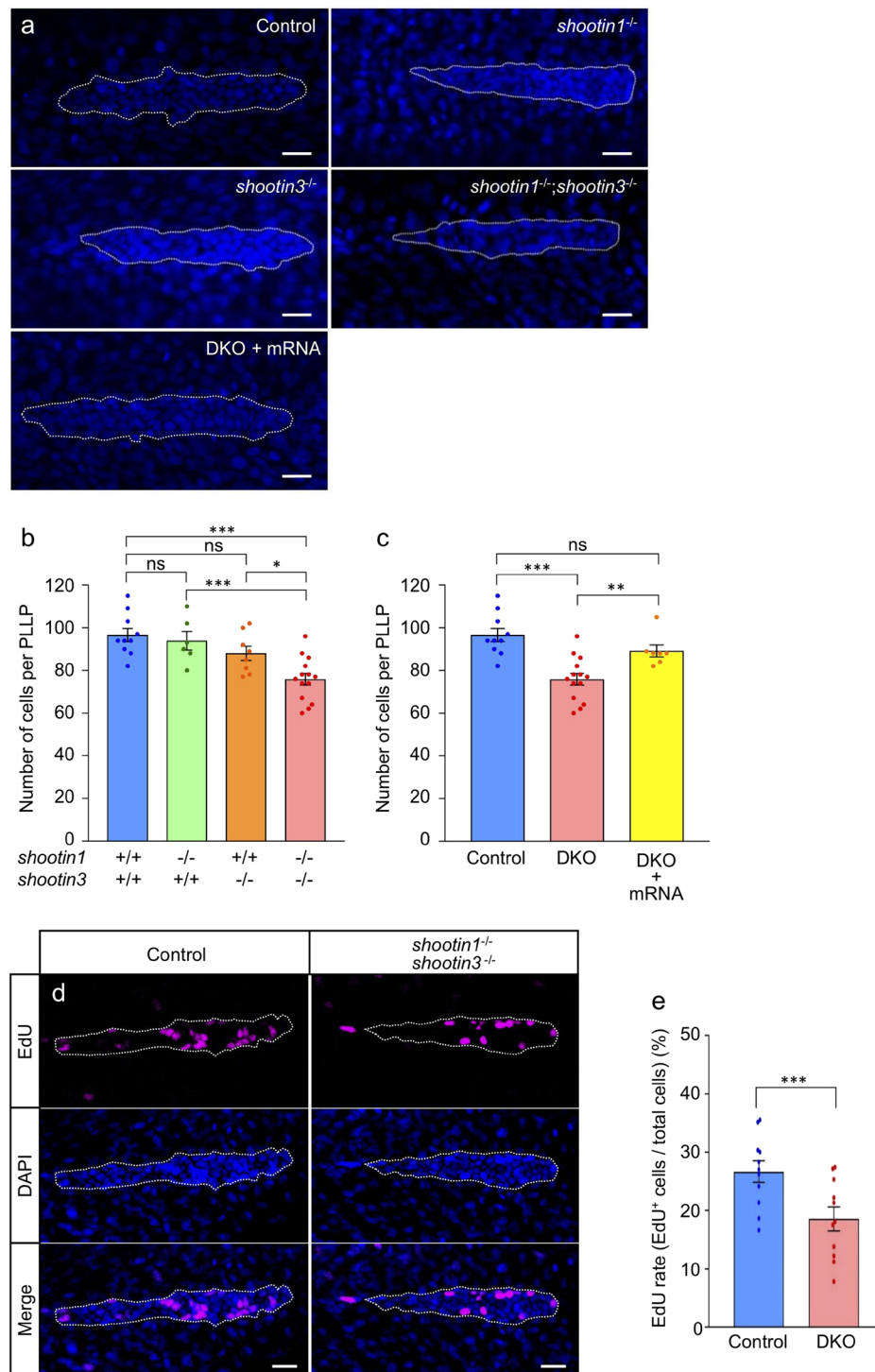


Figure 5. *shootin1;shootin3* double mutants exhibit reduced cell number and reduced cell proliferation in the PLLP. (a) Representative images of DAPI-stained PLLP in wild-type control, *shootin1^{-/-}* single mutant, *shootin3^{-/-}* single mutant and *shootin1^{-/-};shootin3^{-/-}* double mutant embryos at 32 hpf. An image of a PLLP in *shootin1^{-/-};shootin3^{-/-}* double mutant embryo into which *shootin1* and *shootin3* mRNAs were injected is also presented at the bottom. Dotted lines indicate the areas of PLLP, in which small nuclei of PLLP cells cluster. Scale bars: 20 μ m. (b) Number of cells in the PLLP of wild-type control ($n = 10$), *shootin1^{-/-}* single mutant ($n = 6$), *shootin3^{-/-}* single mutant ($n = 8$) and *shootin1^{-/-};shootin3^{-/-}* double mutant ($n = 14$) embryos at 32 hpf obtained from the analyses in (a). (c) Rescue experiments of the reduced cell number of double mutant PLLP cells. The injected DKO embryos (DKO + mRNA, $n = 7$) were analyzed at 32 hpf. Data for the uninjected wild-type (WT) and DKO mutant embryos in (c) are shared with those in (b). (d) Representative images of PLLP stained with EdU and DAPI in wild-type control and *shootin1^{-/-};shootin3^{-/-}* mutant embryos at 32 hpf. Scale bars: 20 μ m. (e) Ratio of EdU-positive cells relative to the total number of cells in the WT ($n = 11$) and DKO mutant ($n = 11$) PLLP at 32 hpf obtained from the analyses in (d). Data in (b), (c) and (e) represent mean \pm SEM; *** $P < 0.01$; * $P < 0.05$; ns, nonsignificant.

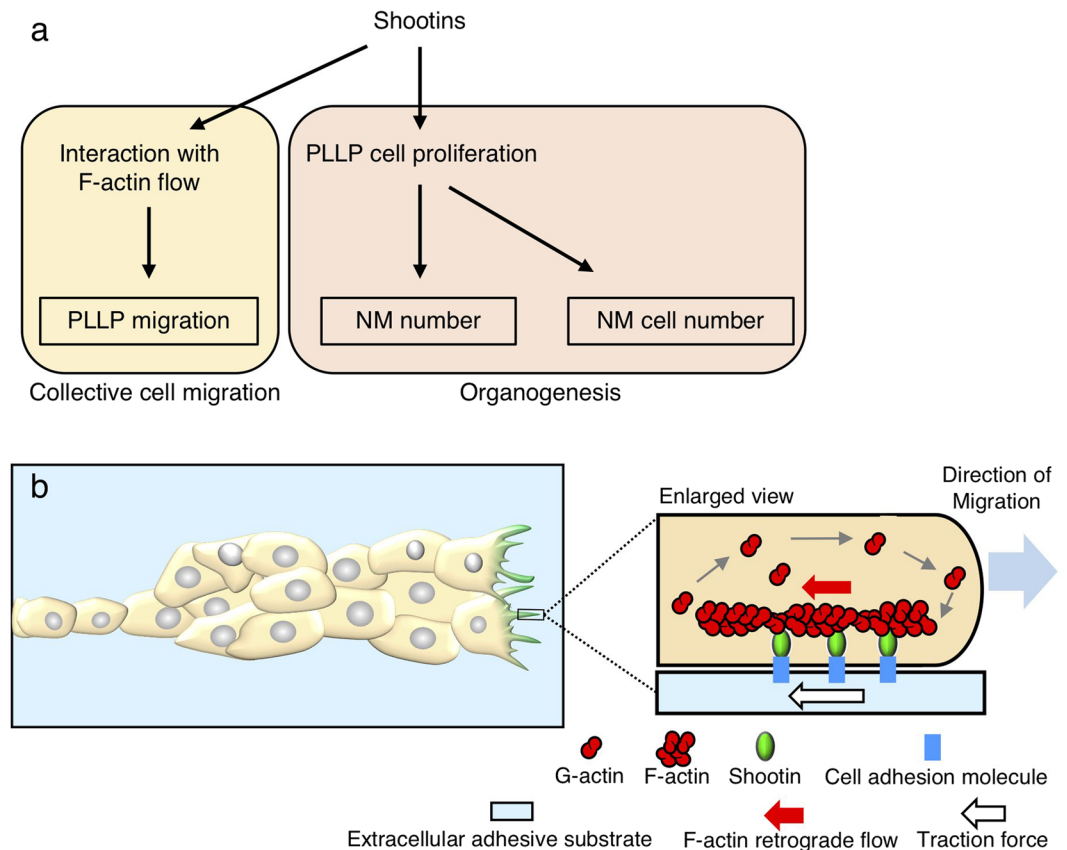


Figure 6. A working model for how shootins mediate collective cell migration and organogenesis of the zebrafish posterior lateral line system. (a) A model for shootin-mediated collective cell migration and organogenesis of the zebrafish posterior lateral line system. Shootins mediate PLLP migration through its interaction with F-actin at the leading edge of the leader cells. Shootins promote cell proliferation in the PLLP, thereby positively regulating the number of neuromasts and the number of cells in the deposited neuromasts. (b) A mechanistic model for shootin1-mediated zebrafish PLLP migration. F-actins polymerize at the filopodia and lamellipodia of PLLP leading cells and depolymerize proximally, thereby inducing retrograde flow of F-actins (red arrow). Shootin1 couples mechanically the F-actin retrograde flow and extracellular adhesive substrates, thereby transmitting the force of F-actin flow (red arrow) to the substrates as a traction force (white arrow)^{31,32,34}. The driving force for PLLP migration (blue arrow) is produced as a counterforce to the traction forces exerted on the extracellular substrates (white arrow).

DNA electrophoresis. The DNA electrophoresis in Fig. 1c and Supplementary Figs S4c and S5c was performed using agarose gels. The images in Fig. 1b were cropped from full-length gel images (Supplementary Fig. S10). All the gel images are raw data without modification.

Whole-mount *in situ* hybridization. Whole-mount *in situ* hybridization was performed as described previously⁵⁶. The following plasmids were constructed for synthesizing *in situ* probes. For constructing pCRII-shootin1, *shootin1* was PCR-amplified using the primers shootin1-h-Ba-Ko and shootin1-r2 and cloned into pCRII-TOPO (Invitrogen). For constructing pGEMT-shootin2, *shootin2* was PCR-amplified with shootin2-h4 and shootin2-r4 and cloned into pGEM-T (Promega). Similarly, to construct pGEMT-shootin3, *shootin3* was PCR-amplified with shootin3-f and shootin3-t-Sp and cloned into pGEM-T (Promega). Plasmids pCRII-shootin1 and pGEMT-shootin3 were digested with SpeI, and antisense probes of *shootin1* and *shootin3* were synthesized using T7 RNA polymerase (Roche). The plasmid pGEMT-shootin2 was digested with SacII, and *shootin2* antisense probes were synthesized using SP6 RNA polymerase (Roche). For constructing pCRII-*atoh1a*, pCRII-*cxcr4b*, pCRII-*cxcr7b* and pCRII-*deltaA*, *atoh1a*, *cxcr4b*, *cxcr7b* and *deltaA* were PCR-amplified with specific primer pairs and cloned into pCRII (Invitrogen). The plasmids pCRII-*atoh1a*, pCRII-*cxcr4b*, pCRII-*cxcr7b* and pCRII-*deltaA* were digested with NotI, and antisense probes of *atoh1a*, *cxcr4b*, *cxcr7b* and *deltaA* were synthesized using SP6 RNA polymerase (Roche). All *in situ* probes were synthesized from cDNAs using the DIG RNA labeling kit (Roche), according to the manufacturer's instructions. Images were acquired with a Leica MZFL III or a Keyence BZ-X700/BZ-X710 microscope and processed using Adobe Photoshop Elements 12 and Fiji⁵⁷.

Fluorescent speckle microscopy. XTC fibroblasts, a cell line established from *Xenopus laevis*⁴⁵, were cultured as described previously⁵⁸ and transfected with pAcGFP-shootin1 or pAcGFP-shootin3 and pmRFP-actin³⁵ using the X-treamGENE 9 transfection reagent (Sigma). Fluorescent speckle imaging was performed as described

previously^{31,32,44}. Images were acquired at 28 °C using an Observer.Z1 fluorescence microscope (Zeiss) equipped with an ORCA-flash4.0 digital CMOS camera (Hamamatsu) and ZEN imaging software (Zeiss). Images were processed using Fiji⁵⁷ and Adobe Photoshop Elements 12 as described previously^{31,32}.

Generation of zebrafish *shootin1* and *shootin3* mutants. Zebrafish mutants of *shootin1* and *shootin3* were generated using the CRISPR/Cas9 system⁵⁹. Vectors for customized guide RNAs (gRNAs) were constructed as described previously⁵⁹. Plasmid pT7-*shootin1* (ex3) was constructed by cloning the two annealed oligonucleotides *shootin1*-f-ex3 and *shootin1*-r-ex3. pT7-*shootin1* (ex4) was constructed by cloning the two annealed oligonucleotides *shootin1*-f-ex4 and *shootin1*-r-ex4, and pT7-*shootin3* (ex2) was constructed by cloning the two annealed oligonucleotides *shootin3*-f-ex2 and *shootin3*-r-ex2. The gRNAs and Cas9 mRNA were synthesized and injected into fertilized eggs as described previously⁵⁹. The injected embryos were raised and crossed with the wild type. To screen *shootin1* and *shootin3* mutants, a T7EI assay was performed as described previously (Supplementary Fig. S6)^{59,60}. We used *shootin1*-5' and *shootin1*-3' primers for *shootin1*, and *shootin3*-5' and *shootin3*-3' primers for *shootin3* (Supplementary Table S1). The PCR products were sequenced using an ABI PRISM3130 (Applied Biosystems). As shown in Supplementary Fig. S10, RT-PCR analyses confirmed that there is no detectable expression of *shootin1* in *shootin1* single mutant or *shootin1*;*shootin3* double mutant embryos. In addition, the expression of *shootin3* was undetectable in *shootin3* single mutant and *shootin1*;*shootin3* double mutant embryos.

Genotyping. PCR-based genotyping was performed to identify *shootin1* mutants. Primers *shootin1* (ex3)-wt and *shootin1* (ex3)-5' were used for screening the wild-type allele of *shootin1* exon 3, and primers *shootin1* (ex3)-mt and *shootin1* (ex3)-5' were used for screening the mutant allele of *shootin1* exon 3. To identify *shootin3* mutations, T7EI-mediated genotyping was performed using the primers *shootin3* (ex3)-5' and *shootin3* (ex3)-3' and two different T7EI assays. The first T7EI assay was performed as described previously (Supplementary Fig. S6a)⁵⁹. In the second T7EI assay, PCR products obtained from samples were mixed with those from the wild type before denaturation at 94 °C for 3 min, annealing at room temperature and digestion of the annealed products with T7EI (Supplementary Fig. S6b)⁶⁰. The first T7EI assay distinguished heterozygous fish from wild-type and homozygous fish, and the second T7EI assay distinguished between homozygous and wild-type fish (Supplementary Fig. S6c)⁶⁰.

Microinjection. Microinjection was performed as described previously⁵⁹. Fertilized eggs were injected with gRNAs (50 pg/embryo) and Cas9 mRNA (300 pg/embryos). In rescue experiments, fertilized eggs were injected with *shootin1* mRNA (25 pg/embryo) and *shootin3* mRNA (25 pg/embryo).

Tissue labeling and microscopy. Embryos were fixed in 4% paraformaldehyde (PFA) in phosphate-buffered saline (PBS: 137 mM NaCl, 2.7 mM KCl, 10 mM Na₂HPO₄, 1.76 mM KH₂PO₄, pH 7.4) overnight at 4 °C. The numbers of cells in the neuromasts and PLLP were counted by DAPI staining as described previously^{18,48,49}. EdU incorporation was performed as described previously⁴⁷. Embryos were dechorionated and 30.5-hpf embryos were immersed in 500 μM EdU solution on ice for 30 min. After washing, embryos were incubated at 28.5 °C for 1 h and fixed at 32 hpf in 4% PFA overnight at 4 °C. The EdU signals were detected using a Click-iT EdU Alexa Fluor488 Imaging Kit (Invitrogen), according to the manufacturer's instructions. Embryos were embedded in 0.5–1% low melting point agarose (Invitrogen). Confocal images were captured with a Zeiss LSM700 or Zeiss LSM710 microscope and processed using Adobe Photoshop Elements 12 and Fiji⁵⁷.

Statistical analysis. Results are expressed as mean ± standard error (SEM). Statistical analyses were performed with GraphPad Prism 7. Statistical significance was determined by the two-tailed unpaired Student's *t*-test. For multiple comparisons, we used one-way ANOVA with Tukey's *post hoc* test.

References

- Ghysen, A. & Dambly-Chaudiere, C. The lateral line microcosmos. *Genes Dev* **21**, 2118–2130 (2007).
- Aman, A. & Piotrowski, T. Cell-cell signaling interactions coordinate multiple cell behaviors that drive morphogenesis of the lateral line. *Cell Adh Migr* **5**, 499–508 (2011).
- Ma, E. Y. & Raible, D. W. Signaling pathways regulating zebrafish lateral line development. *Curr Biol* **19**, R381–386 (2009).
- Aman, A. & Piotrowski, T. Cell migration during morphogenesis. *Dev Biol* **341**, 20–33 (2010).
- Lopez-Schier, H. Fly fishing for collective cell migration. *Curr Opin Genet Dev* **20**, 428–432 (2010).
- Wada, H. & Kawakami, K. Size control during organogenesis: Development of the lateral line organs in zebrafish. *Dev Growth Differ* **57**, 169–178 (2015).
- Aman, A. & Piotrowski, T. Multiple signaling interactions coordinate collective cell migration of the posterior lateral line primordium. *Cell Adh Migr* **3**, 365–368 (2009).
- Chitnis, A. B., Nogare, D. D. & Matsuda, M. Building the posterior lateral line system in zebrafish. *Dev Neurobiol* **72**, 234–255 (2012).
- Gasparov, E. V., Rafieva, L. M. & Korzh, V. P. BDNF-TrkB axis regulates migration of the lateral line primordium and modulates the maintenance of mechanoreceptor progenitors. *PLoS One* **10**, e0119711 (2015).
- Li, Q., Shirabe, K. & Kuwada, J. Y. Chemokine signaling regulates sensory cell migration in zebrafish. *Dev Biol* **269**, 123–136 (2004).
- Haas, P. & Gilmour, D. Chemokine signaling mediates self-organizing tissue migration in the zebrafish lateral line. *Dev Cell* **10**, 673–680 (2006).
- Dambly-Chaudiere, C., Cubedo, N. & Ghysen, A. Control of cell migration in the development of the posterior lateral line: antagonistic interactions between the chemokine receptors CXCR4 and CXCR7/RDC1. *BMC Dev Biol* **7**, 1–14 (2007).
- Valentin, G., Haas, P. & Gilmour, D. The chemokine SDF1a coordinates tissue migration through the spatially restricted activation of Cxcr7 and Cxcr4b. *Curr Biol* **17**, 1026–1031 (2007).
- Dona, E. *et al.* Directional tissue migration through a self-generated chemokine gradient. *Nature* **503**, 285–289 (2013).
- Venkiteswaran, G. *et al.* Generation and dynamics of an endogenous, self-generated signaling gradient across a migrating tissue. *Cell* **155**, 674–687 (2013).

16. Harding, M. J., McGraw, H. F. & Nechiporuk, A. The roles and regulation of multicellular rosette structures during morphogenesis. *Development* **141**, 2549–2558 (2014).
17. Aman, A. & Piotrowski, T. Wnt/beta-catenin and Fgf signaling control collective cell migration by restricting chemokine receptor expression. *Dev Cell* **15**, 749–761 (2008).
18. Kozlovskaja-Gumbriene, A. *et al.* Proliferation-independent regulation of organ size by Fgf/Notch signaling. *eLife* **6**, 1–31 (2017).
19. Haeger, A., Wolf, K., Zegers, M. M. & Friedl, P. Collective cell migration: guidance principles and hierarchies. *Trends Cell Biol* **25**, 556–566 (2015).
20. Friedl, P. & Gilmour, D. Collective cell migration in morphogenesis, regeneration and cancer. *Nat Rev Mol Cell Biol* **10**, 445–457 (2009).
21. Svitkina, T. The actin cytoskeleton and actin-based motility. *Cold Spring Harb Perspect Biol* **10** (2018).
22. Hirata, H., Sokabe, M. & Lim, C. T. Molecular mechanisms underlying the force-dependent regulation of actin-to-ECM linkage at the focal adhesions. *Prog Mol Biol Transl Sci* **126**, 135–154 (2014).
23. Suter, D. M. & Forscher, P. Substrate-cytoskeletal coupling as a mechanism for the regulation of growth cone motility and guidance. *J Neurobiol* **44**, 97–113 (2000).
24. Lowery, L. A. & Van Vactor, D. The trip of the tip: understanding the growth cone machinery. *Nat Rev Mol Cell Biol* **10**, 332–343 (2009).
25. Pollard, T. D. & Borisy, G. G. Cellular motility driven by assembly and disassembly of actin filaments. *Cell* **112**, 453–465 (2003).
26. Toriyama, M. *et al.* Shootin1: a protein involved in the organization of an asymmetric signal for neuronal polarization. *J Cell Biol* **175**, 147–157 (2006).
27. Higashiguchi, Y. *et al.* Identification of a shootin1 isoform expressed in peripheral tissues. *Cell Tissue Res* **366**, 75–87 (2016).
28. Inagaki, N., Toriyama, M. & Sakumura, Y. Systems biology of symmetry breaking during neuronal polarity formation. *Dev Neurobiol* **71**, 584–593 (2011).
29. Sapir, T. *et al.* Shootin1 acts in concert with KIF20B to promote polarization of migrating neurons. *J Neurosci* **33**, 11932–11948 (2013).
30. Abe, K. *et al.* Grip and slip of L1-CAM on adhesive substrates direct growth cone haptotaxis. *Proc Natl Acad Sci USA* **115**, 2764–2769 (2018).
31. Shimada, T. *et al.* Shootin1 interacts with actin retrograde flow and L1-CAM to promote axon outgrowth. *J Cell Biol* **181**, 817–829 (2008).
32. Kubo, Y. *et al.* Shootin1-cortactin interaction mediates signal-force transduction for axon outgrowth. *J Cell Biol* **210**, 663–676 (2015).
33. Toriyama, M., Kozawa, S., Sakumura, Y. & Inagaki, N. Conversion of a signal into forces for axon outgrowth through Pak1-mediated shootin1 phosphorylation. *Curr Biol* **23**, 529–534 (2013).
34. Baba, K. *et al.* Gradient-reading and mechano-effector machinery for netrin-1-induced axon guidance. *eLife* **7**, e34593 (2018).
35. Katsuno, H. *et al.* Actin migration driven by directional assembly and disassembly of membrane-anchored actin filaments. *Cell Rep* **12**, 648–660 (2015).
36. Inagaki, N. & Katsuno, H. Actin waves: origin of cell polarization and migration? *Trends Cell Biol* **27**, 515–526 (2017).
37. Minegishi, T. *et al.* Shootin1b mediates a mechanical clutch to produce force for neuronal migration. *Cell Rep* **25**, 624–639 (2018).
38. Emerson, S. E. *et al.* Identification of target genes downstream of semaphorin6A/PlexinA2 signaling in zebrafish. *Dev Dyn* **246**, 539–549 (2017).
39. Amores, A. *et al.* Zebrafish hox clusters and vertebrate genome evolution. *Science* **282**, 1711–1714 (1998).
40. Meyer, A. & Malaga-Trillo, E. Vertebrate genomics: More fishy tales about Hox genes. *Curr Biol* **9**, R210–213 (1999).
41. Meyer, A. & Schartl, M. Gene and genome duplications in vertebrates: the one-to-four (-to-eight in fish) rule and the evolution of novel gene functions. *Curr Opin Cell Biol* **11**, 699–704 (1999).
42. Aparicio, S. Vertebrate evolution: recent perspectives from fish. *Trends Genet* **16**, 54–56 (2000).
43. Naruse, K. *et al.* A detailed linkage map of medaka, *Oryzias latipes*: comparative genomics and genome evolution. *Genetics* **154**, 1773–1784 (2000).
44. Watanabe, N. & Mitchison, T. J. Single-molecule speckle analysis of actin filament turnover in lamellipodia. *Science* **295**, 1083–1086 (2002).
45. Pudney, M., Varma, M. G. & Leake, C. J. Establishment of a cell line (XTC-2) from the South African clawed toad, *Xenopus laevis*. *Experientia* **29**, 466–467 (1973).
46. Muto, A. *et al.* Genetic visualization with an improved GCaMP calcium indicator reveals spatiotemporal activation of the spinal motor neurons in zebrafish. *Proc Natl Acad Sci USA* **108**, 5425–5430 (2011).
47. Agarwala, S. *et al.* Amotl2a interacts with the Hippo effector Yap1 and the Wnt/beta-catenin effector Lef1 to control tissue size in zebrafish. *eLife* **4**, e08201 (2015).
48. Aman, A., Nguyen, M. & Piotrowski, T. Wnt/beta-catenin dependent cell proliferation underlies segmented lateral line morphogenesis. *Dev Biol* **349**, 470–482 (2011).
49. He, Y. *et al.* Insm1a Is Required for Zebrafish Posterior Lateral Line Development. *Front Mol Neurosci* **10**, 241 (2017).
50. McGraw, H. F. *et al.* Lef1 is required for progenitor cell identity in the zebrafish lateral line primordium. *Development* **138**, 3921–3930 (2011).
51. Valdivia, L. E. *et al.* Lef1-dependent Wnt/beta-catenin signalling drives the proliferative engine that maintains tissue homeostasis during lateral line development. *Development* **138**, 3931–3941 (2011).
52. Xu, H. *et al.* Gbeta1 controls collective cell migration by regulating the protrusive activity of leader cells in the posterior lateral line primordium. *Dev Biol* **385**, 316–327 (2014).
53. Urasaki, A., Morvan, G. & Kawakami, K. Functional dissection of the Tol2 transposable element identified the minimal cis-sequence and a highly repetitive sequence in the subterminal region essential for transposition. *Genetics* **174**, 639–649 (2006).
54. Letunic, I. & Bork, P. 20 years of the SMART protein domain annotation resource. *Nucleic Acids Res* **46**, D493–D496 (2018).
55. Saitou, N. & Nei, M. The neighbor-joining method: a new method for reconstructing phylogenetic trees. *Mol Biol Evol* **4**, 406–425 (1987).
56. Schulte-Merker, S. Looking at embryos. In zebrafish: a practical approach. *New York, NY Oxford Univ. Press*, 39–58 (2002).
57. Schindelin, J. *et al.* Fiji: an open-source platform for biological-image analysis. *Nat Methods* **9**, 676–682 (2012).
58. Higashida, C. *et al.* Actin polymerization-driven molecular movement of surfacemDia1 in living cells. *Science* **303**, 2007–2010 (2004).
59. Jao, L. E., Wentz, S. R. & Chen, W. Efficient multiplex biallelic zebrafish genome editing using a CRISPR nuclease system. *Proc Natl Acad Sci USA* **110**, 13904–13909 (2013).
60. Huang, L., Urasaki, A. & Inagaki, N. Rab33a and Rab33b mediate the outgrowth of forebrain commissural axons in the zebrafish brain. *Sci Rep* **9**, 1799 (2019).

Acknowledgements

We thank Maiko Yokouchi, Hiroko Shigesato and Mieko Ueda for maintaining the zebrafish, Drs Kentarou Baba and Takunori Minegishi for technical support, Drs Kenichi Takano and Matthew Holly for providing materials, and Dr. Yuichi Sakumura and all the members of Inagaki lab for helpful discussions. This research was supported in part by a JSPS Grant-in-Aid for Scientific Research on Innovative Areas (JP25102010), JSPS KAKENHI (JP23370088, JP26290007 and JP 26840081), AMED under Grant Number JP19gm0810011, the Foundation for Nara Institute of Science and Technology, the National BioResource Project (NBRP) from AMED and the Takeda Science Foundation.

Author Contributions

A.U. and N.I. conceived and designed the experiments. A.U., S.M., K.N., S.M., M.U., K.A., L.H. and E.W. conducted the experiments and analyzed data. K.K. provided the SAIGFF213A line. O.N., T.M. and Y.B. supported the experiments with technical advice and useful discussions. A.U. and N.I. wrote the manuscript. All authors reviewed the manuscript.

Additional Information

Supplementary information accompanies this paper at <https://doi.org/10.1038/s41598-019-48585-4>.

Competing Interests: The authors declare no competing interests.

Publisher's note: Springer Nature remains neutral with regard to jurisdictional claims in published maps and institutional affiliations.



Open Access This article is licensed under a Creative Commons Attribution 4.0 International License, which permits use, sharing, adaptation, distribution and reproduction in any medium or format, as long as you give appropriate credit to the original author(s) and the source, provide a link to the Creative Commons license, and indicate if changes were made. The images or other third party material in this article are included in the article's Creative Commons license, unless indicated otherwise in a credit line to the material. If material is not included in the article's Creative Commons license and your intended use is not permitted by statutory regulation or exceeds the permitted use, you will need to obtain permission directly from the copyright holder. To view a copy of this license, visit <http://creativecommons.org/licenses/by/4.0/>.

© The Author(s) 2019